ELSEVIER

Microelectronics Reliability 44 (2004) 237–243

MICROELECTRONICS
RELIABILITY

www.elsevier.com/locate/microrel

Fabrication of suspended thin film resonator for application of RF bandpass filter

Hyun Ho Kim [a,*], Byeong Kwon Ju [b], Yun Hi Lee [b], Si Hyung Lee [c], Jeon Kook Lee [c], Soo Won Kim [a]

[a] *Department of Electronics Engineering, Korea University, 5-1, Anam-dong Sungbuk-ku, Seoul 136-701, South Korea*
[b] *Microsystem Research Center, KIST, 39-1, Hawolgok-dong, Seongbuk-gu, Seoul 136-791, South Korea*
[c] *Thin Film Technology Research Center, KIST, 39-1, Hawolgok-dong, Seongbuk-gu, Seoul 136-791, South Korea*

Received 16 October 2002; received in revised form 1 September 2003

Abstract

Characteristics of AlN thin film and thin film resonator for RF bandpass filter have been studied. AlN thin films were deposited by RF magnetron sputter system. Deposition parameters such as N_2 contents, Ar and N_2 partial pressures, and the distance between metal target and substrate were found to affect the piezoelectric response. To fabricate the suspended thin film resonator (STFR) using the piezoelectric AlN thin film, the etching of AlN and the surface micromachining process were conducted. The thickness of AlN film and membrane for the STFR are 2 and 15 μm, respectively. This membrane was fabricated by SOI technology. The device with the dimension of 160×160 μm^2 has a resonant frequency of 1.653 GHz, a K^2_{eff} of 2.4%, a bandwidth of 17 MHz, and a quality factor of 91.7. The device with the dimension of 200×200 μm^2 has a resonant frequency of 1.641 GHz, a K^2_{eff} of 1.2%, and a bandwidth of 9 MHz, and a quality factor of 50.2.

© 2003 Published by Elsevier Ltd.

1. Introduction

There have been studies to use piezoelectric thin films as a component material for sensors and actuators. In particular, characteristics of frequency and impedance in RF filter of wireless communication systems are related to piezoelectric thin films such as AlN and ZnO. The critical factor of piezoelectric thin films is the *c*-axis orientation and the lattice parameter because of the vibration of thickness mode. Every portable product such as pager, cellular phone, navigation, satellite communication, and various forms of data communication operating high frequency requires the use of a bandpass filter to selectively transmit signals within the passband. Thin film resonator (TFR) has advantages of small size, low power, low insertion loss, bandpass filter with high frequency, and good bandwidth [1–6].

TFR consisting in piezoelectric thin film between two electrodes uses the standing wave formed by electromechanical coupling of piezoelectric characteristic. The boundary between the substrate and the bottom electrode in order to form the standing wave must satisfy the condition of air or vacuum. In order to satisfy the boundary condition, many researches for TFR with free standing membrane fabricated by microelectromechanical system (MEMS) technology have been studied [7–9].

In this paper, characteristics of AlN piezoelectric thin film are inspected and the suspended type thin film resonators (STFRs) using SOI technology are fabricated with the AlN piezoelectric thin film on Si (15 μm) membrane. AlN piezoelectric thin film is deposited by RF magnetron sputter system. This membrane is freestanding to acoustically isolate from the Si substrate. The process was designed to be compatible with a silicon-integrated process.

---

[*] Corresponding author. Tel.: +82-32-500-1815; fax: +82-32-544-1493.
E-mail address: hkim@bsecm.com (H.H. Kim).

0026-2714/$ - see front matter © 2003 Published by Elsevier Ltd.
doi:10.1016/j.microrel.2003.09.007

2. Experimental

2.1. Characteristics of AlN

The crystallization of AlN thin film is depended on the equipment and the condition of environment. All of deposition variables focus on the *c*-axis orientation. Deposition variables are N_2 contents, Ar and N_2 partial pressures, the distance between metal target and substrate and RF power. In the experiment result, the 20% reduction of N_2 contents is increased the (0 0 2) orientation and the distance variation between target and substrate from 6 to 10 cm shows the variation of the *c*-axis orientation in AlN layer. Fig. 1(a) shows the XRD result of AlN crystallographic variation dependent on the deposition pressure and the distance between target and substrate. In Fig. 1(a), the minimum distance between target and substrate and the deposition pressure for the (0 0 2) orientation of AlN thin film are 6 cm and 1–10 mTorr, respectively. Fig. 1(b) shows SEM micrographs of the surface morphology and the cross-section of AlN thin film deposited with the optimum condition. Fig. 1(b) shows the columnar structure from the cross-section of AlN. In this figure, the average grain size is about 60 nm, and the deposition rate is 13 nm/min. Fig. 2 shows FT-IR spectrum and dielectric properties of the *c*-axis oriented AlN. The result of Fig. 2(b) analyzed with the HP 4194A impedance analyzer. The relative

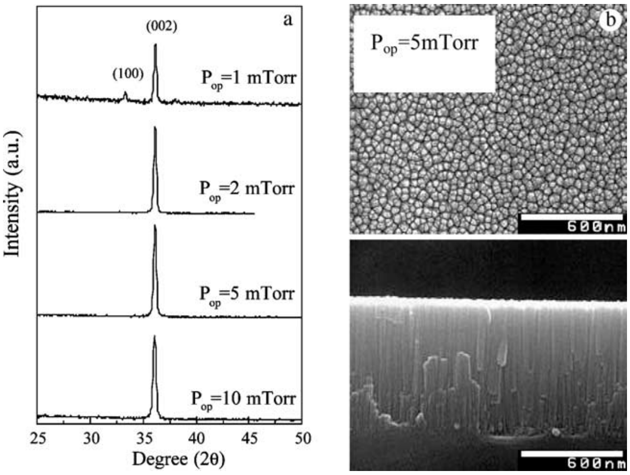

Fig. 1. Highly *c*-axis (0 0 2) oriented AlN thin film on Si (1 0 0) substrate by RF magnetron sputtering without substrate heating. (High deposition rate ≅ 13 nm/min).

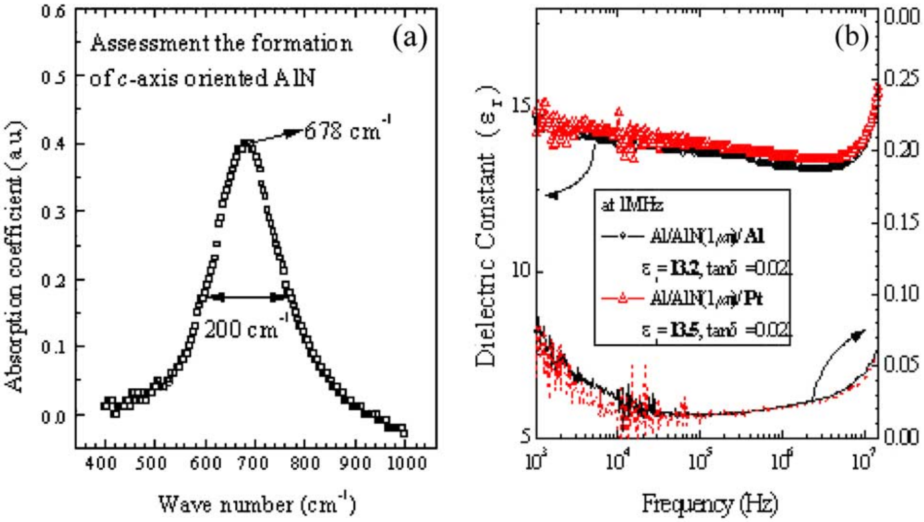

Fig. 2. FT-IR spectrum and dielectric properties of highly *c*-axis (0 0 2) oriented AlN thin film on Si (1 0 0) substrate.

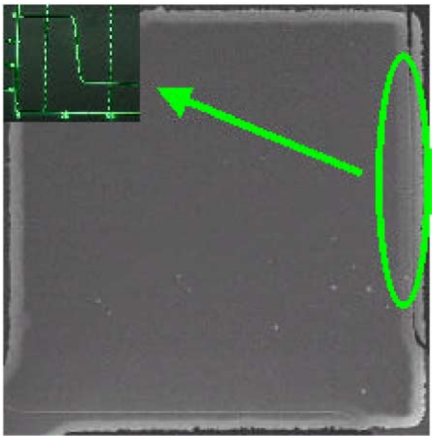

Fig. 3. SEM micrograph of pattern etched by a dilute TMAH etchant.

dielectric constant is 13.2 at 1 MHz and the loss tangent is 0.021. It shows higher result than the dielectric constant ($\varepsilon r = 8.5$) of polycrystalline AlN because of the *c*-axis orientation [10–12].

The AlN etch is the important process because the resonances of thin film bulk acoustic resonators are determined by the thickness of the AlN piezoelectric between the two reflecting surfaces. Unfortunately, all the known AlN etchants attack aluminum, so passivation layers need to be employed. We used a dilute TMAH solution of 0.6 wt.% in order to protect the overetch of pattern. At room temperature, the AlN etch rate was 200 nm/min. Advantages of this etch are a good coverage, the etch at room temperature, and the simplicity. Fig. 3 shows SEM micrograph after AlN etch.

2.2. Process of suspended thin film resonator

Suspended type thin film bulk acoustic resonators (STFRs) are fabricated using surface micromachining technologies. Fig. 4 shows photographs of 15 μm suspended membrane. This was formed by using Si/SiO_2 (15 μm/1 μm) SOI wafer. Fig. 5 shows cross-section view of STFR and SEM micrographs of the suspended membrane. Initially, a Si/SiO_2 (15 μm/1 μm) SOI wafer was prepared. The pattern of window open was formed. The 15 μm membrane by etching 1 μm SiO_2 was formed. For the STFR, the resonating stack is supported by silicon membrane. Since silicon membrane is part of the resonating stack, its properties strongly affect the resonator K_{eff}^2 and Q. All layers within the acoustic stack play a role in determining the frequencies of the resonating modes. The roughness of all layers within the acoustic stack influenced the device Q because the device Q is a measure of loss within the device. This loss can

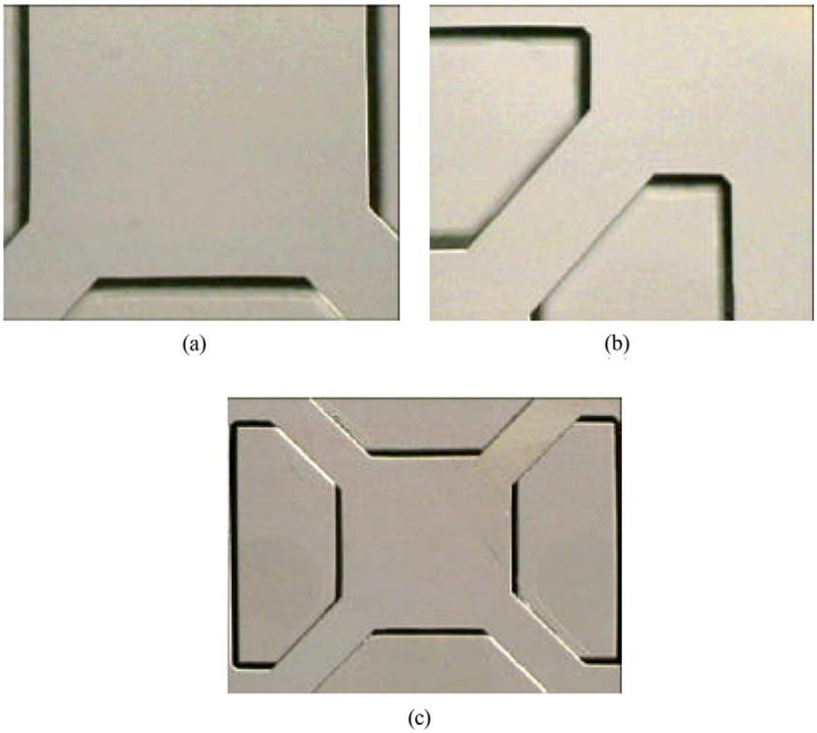

Fig. 4. Photographs of 15 μm suspended membrane (top view).

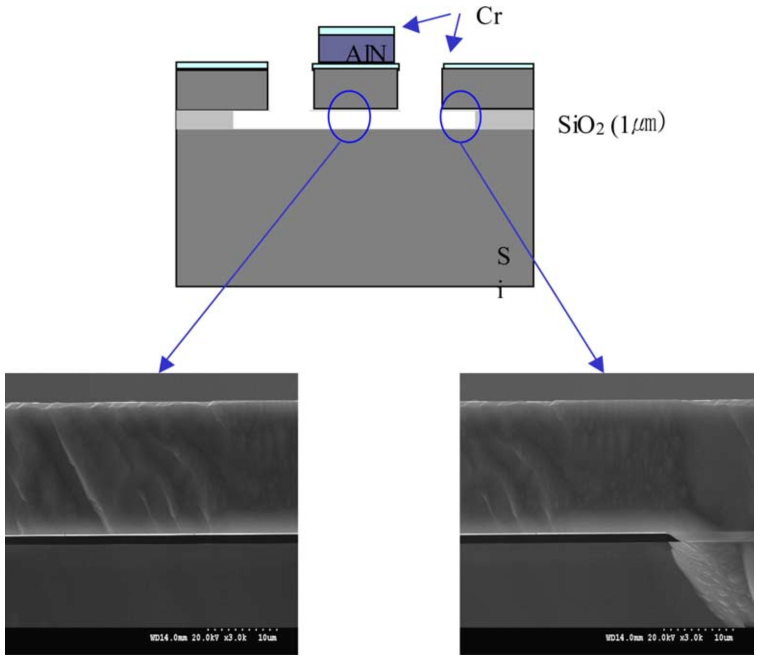

Fig. 5. Cross-section view STER and SEM micrographs of the suspended membrane.

Sample	Rms	Ave
Membrane front	65.1Å	48.4Å
Membrane back	6.49Å	3.38Å
Si	2.90Å	1.82Å

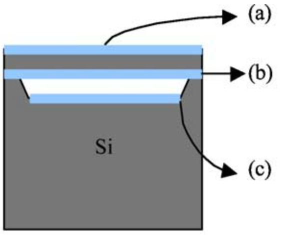

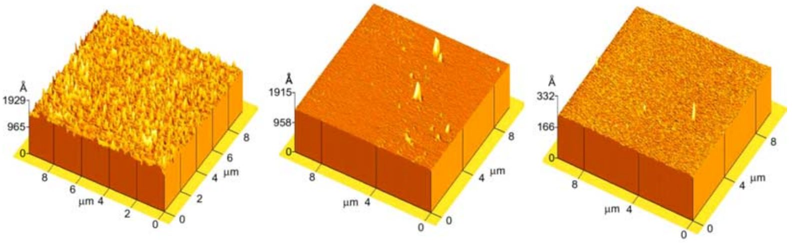

(a) Membrane Front (b) Membrane Back (c) Si

Fig. 6. AFM micrographs for surface roughness of the suspended membrane.

result from acoustic loss within the acoustic stack, scattering of the acoustic waves from rough surfaces or grain boundaries, and acoustic radiation into the surrounding area of the device. Fig. 6 shows AFM measurement results of surface roughness for the suspended membrane. The average roughness of membrane front and membrane back is 48.4 and 3.38 Å, respectively. The roughness of membrane front compared to Si roughness is large. From this result, we can know that the roughness of membrane front is much affected in the loss of membrane. However, if it is compared to AlN roughness, this result can be ignored. Cr thin film (3000 Å) as the bottom electrode was deposited by using thin-film sputtering techniques. Although several researchers have used Al thin film as the electrode, we used Cr thin film because Al thin film was etched by the etchant of AlN piezoelectric thin film. This process was reduced the unnecessary process such as the passivation layer for the

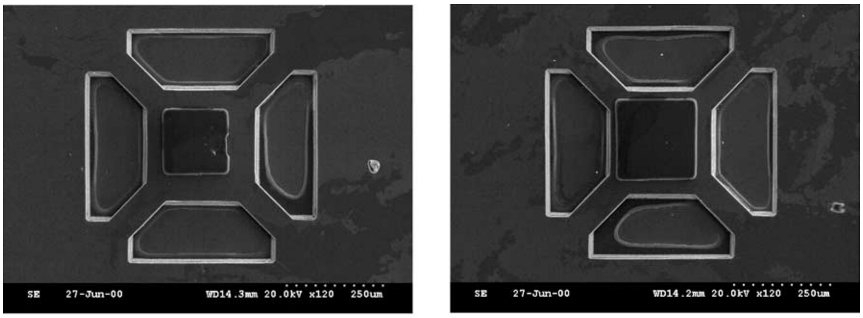

(a)160μm×160μm (b) 200μm×200μm

Fig. 7. SEM microscopes of the fabricated STFR.

bottom electrode. The 2 μm AlN piezoelectric film was deposited on top of the Cr bottom electrode using an RF magnetron sputtering system. After the deposition of the piezoelectric AlN, the top electrode was deposited Cr thin film (3000 Å) in the same way on the AlN thin film. The top electrode and the piezoelectric AlN were etched and patterned. The AlN thin film piezoelectric was etched using a dilute TMAH etchant. STFRs are suspended from the silicon substrate and have an air-gap for acoustically reflecting surfaces. Fig. 7 shows SEM microscopes of the fabricated STFR.

3. Results and discussion

The STFR structures were tested in a one-port configuration. The one-port results were obtained using a HP 8510C network analyzer and a ground-signal-ground type probe station. For every measurement sequence, the RF probing system was calibrated over a selected frequency range from 0.5 to 4 GHz. Fig. 8 shows measured wideband response of the reflection coefficient dependent on the respective dimension of 160×160 μm^2 and 200×200 μm^2. The area of the top electrode determines the active area of the TFR device. In Fig. 8, it can know the difference of measured responses dependent on the active area because the capacitive impedance of the active area underneath the electrode is related to the broadband capacitance value and the total capacitance of AlN piezoelectric layer depends on the dimension of the top electrode. Fig. 9 shows measured results of the S_{11} narrowband response in a low point for the respective dimension. The reflection coefficient (S_{11}) of −19.3 dB at 1.653 GHz of the resonance frequency in Fig. 9(a) was obtained. In Fig. 9(b), the reflection coefficient (S_{11}) of −26.1 dB at 1.641 GHz of the resonance frequency was also obtained. The interval between the resonance frequencies was 220 MHz.

Fig. 10 shows measured narrowband response of the input impedance for the STFR. This graph has a local impedance maximum and impedance minimum. The frequency of the minimum is called the series resonance

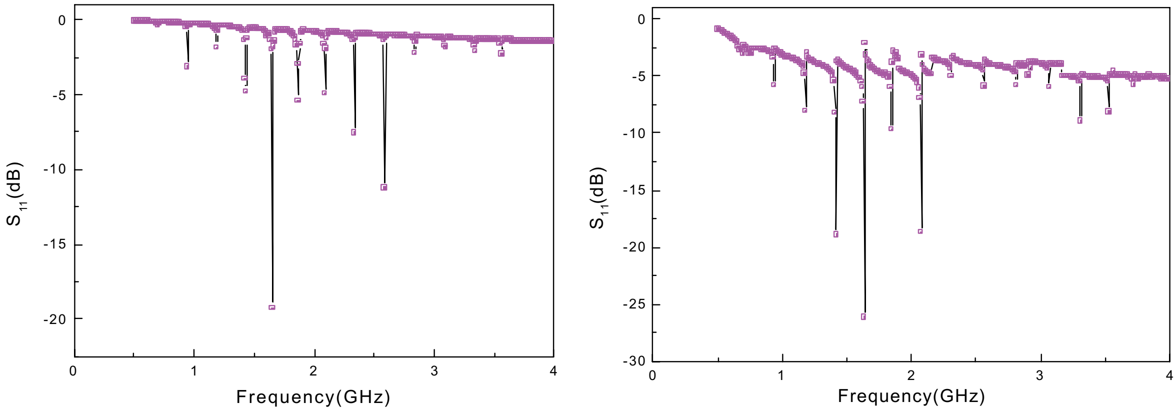

(a)160μm×160μm (b) 200μm×200μm

Fig. 8. Measured wideband response of the reflection coefficient dependent on the respective dimension of 160×160 μm^2 and 200×200 μm^2.

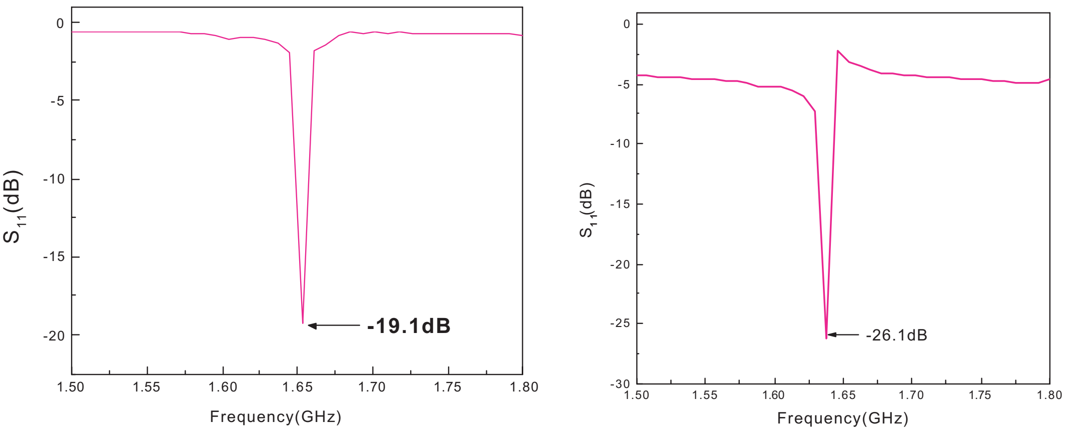

(a)160μm×160μm

(b) 200μm×200μm

Fig. 9. Measured results of the S_{11} narrowband response for the respective dimension.

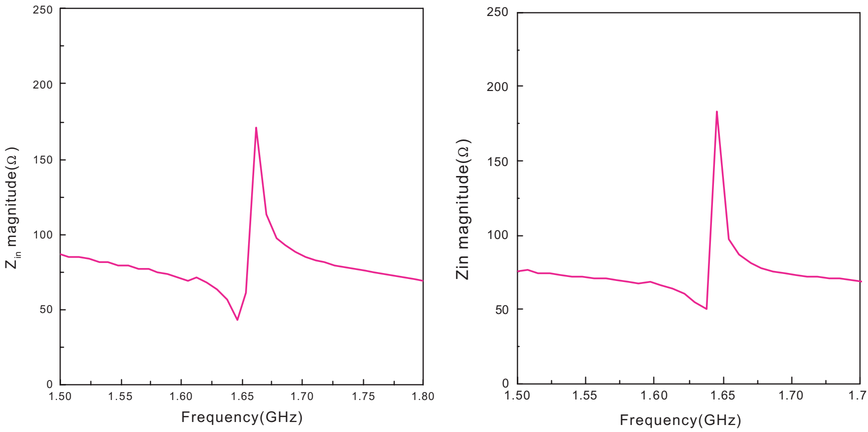

(a)160μm×160μm

(b) 200μm×200μm

Fig. 10. Measured narrowband response of the input impedance for the STFR.

(fs) and the frequency of the maximum is the parallel resonance (fp). In the dimension of 160×160 μm^2, the series resonance and the parallel resonance were 1.645 and 1.662 GHz, respectively. In the dimension of 200×200 μm^2, the series resonance and the parallel resonance were 1.637 and 1.646 GHz, respectively. The separation of the resonances can be related to the piezoelectric, electric, and mechanical properties of the material. For the impedance characteristics, the effective electromechanical coupling coefficient is defined [13]. K^2_{eff} is a measure of the relative frequency spacing between the series and parallel resonance and ultimately determines the maximum bandwidth. The effective electromechanical coupling coefficient (K^2_{eff}) is 2.4% and the bandwidth is 17 MHz for this device with the dimension of 160×160 μm^2. The effective electromechanical coupling coefficient (K^2_{eff}) is 1.2% and the bandwidth is 9 MHz for this device with the dimension of 200×200 μm^2.

Fig. 11 shows measured narrowband phase response of the input impedance for the STFR. The phase response can be differentiated, and the quality factor (Q) of the device can be extracted [13]. The Q of a resonance is a measure of the acoustic loss in the device. It is essential that f_s and f_p are defined because both K^2_{eff} and Q are sensitive functions of f_s and f_p. The frequencies of maximum phase slope can also be used to define the series and parallel resonance. In Fig. 11(a), the series quality factor (Q_s) and the parallel quality factor (Q_p) are 91.7 and 87.7, respectively. In Fig. 11(b), the series quality factor (Q_s) and the parallel quality factor (Q_p) are 50.2 and 63.2, respectively.

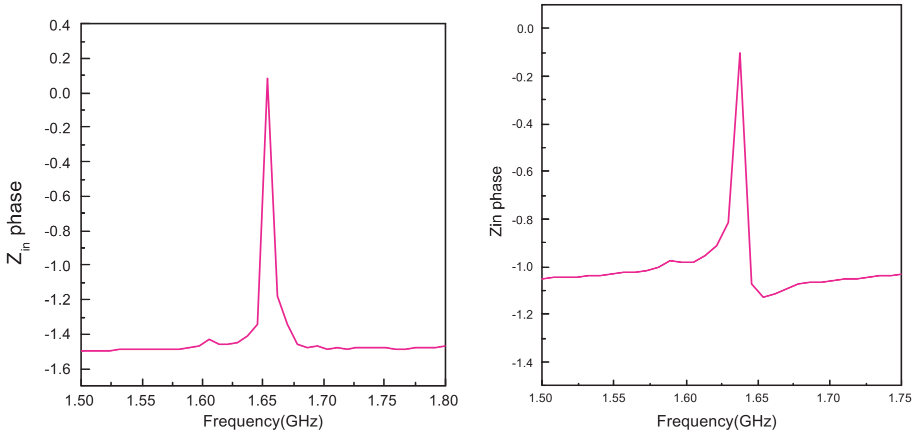

(a) 160μm×160μm (2) 200μm×200μm

Fig. 11. Measured narrowband phase response of the input impedance for the STFR.

4. Conclusions

AlN as the piezoelectric material was deposited by RF magnetron sputter system. Deposition parameters such as N_2 contents, Ar and N_2 partial pressures, and the distance between metal target and substrate were investigated. The STFR was fabricated and measured. The membrane release using SOI technology increases the manufacturability of the process by reducing the potential for a TFR to stick to the underlying substrate and the simplicity of the process. The AlN etch applied this paper produce highly an improvement of the process in terms of time consumption and etch profile. The device with the dimension of 160×160 μm^2 has a resonant frequency of 1.653 GHz, a K^2_{eff} of 2.4%, a bandwidth of 17 MHz, and a quality factor of 91.7. The device with the dimension of 200×200 μm^2 has a resonant frequency of 1.641 GHz, a K^2_{eff} of 1.2%, and a bandwidth of 9 MHz, and a quality factor of 50.2. This device has advantages of integration, mass production, small size, and low cost compared to the previously used resonators. The STFR process is compatible with active silicon devices and was developed integrated RF bandpass filters.

References

[1] Lakin KM. Modeling of thin film resonators and filters. In: Proc IEEE MTT-Int Microwave Symp Dig, June 1992. p. 149–52.

[2] Lakin KM, Kline GR, McCarron KT. High-*Q* microwave acoustic resonators and filters. IEEE Trans Microwave Theory Tech 1993;41(12):2139–46.

[3] Lakin KM, Kline GR, McCarron KT. Development of miniature filters for wireless applications. IEEE Trans Microwave Theory Tech 1995;43(12):2933–9.

[4] Horwitz S, Milton C. Application of film bulk acoustic resonators. In: Proc IEEE MTT-S Int Microwave Symp Dig, June 1992. p. 165–8.

[5] Krishnaswamy SV, Rosenbaum JF, Horwitz SS, Vale C, Moore RA. Compact FBAR filters offer low-loss performance. Microwave RF 1991:127–35.

[6] Naik RS, Lutsky JJ, Rief R, Sodini CG. Electromechanical coupling constant extraction of thin-film piezoelectric materals using a bulk acoustic wave resonator. IEEE Trans Ultrason Ferroelectr Freq Control 1998;45(1).

[7] Kim S-H, Lee J-S, Choi H-C, Lee Y-H. Fabrication of thin-film bulk acoustic wave resonators employing a ZnO/Si composite diaphragm structure using porous silicon layer etching. IEEE Electron Dev Lett 1999;20(3).

[8] Yoshimoto S, Sakamoto M, Hashimoto K, Yamaguchi M. Multi-layered ultrasonic transducers employing air-gap structure. IEEE Trans Ultrason Ferroelectr Freq Control 1995;42(3).

[9] Guckel H, Larsen S, Lagally MG, Moore G, Miller JB, Wiley JD. Electromechanical devices utilizing thin Si diaphragms. Appl Phys 1977;31(9).

[10] Dubois MA, Muralt P. Properties of aluminum nitride thin films for piezoelectric transducers and microwave filter applications. Appl Phys Lett 1999;74(20).

[11] Liufu D, Kao KC. Piezoelectric, dielectric, and interfacial properties of aluminum nitride films. J Vac Sci Technol A 1998;16(4).

[12] Imori M, Taniguchi T, Matsumoto H, Sakai T. A photomultiplier high voltage power supply incorporating a piezoelectric ceramic transformer. IEEE Trans Nucl Sci 1996;43(3).

[13] Rosenbaum J. Bulk acoustic wave theory and devices. Norwood, Mass: Artech House, Inc; 1988.